An Efficient Industrial Robot Calibrator with Multi-Planer Constraints
Supplementary Material

Anonymous

This is the supplementary file for the paper, where the convergence proof of the AMPC algorithm is provided. Moreover, additional tables and figures regarding the symbol appointment, model parameters, experimental process and results and the MCS-AMPC's pseudocode are placed here.

I. Additional Tables

TABLE S.I. Symbol list.

Symbol	Explanation
$\mathbb{R}_i$	Transformation matrix.
a, θ, α, d	Link length, joint angle, link twist angle, link offset.
H, S	Nominal position matrix, Nominal rotation vector.
$\Delta\mathbb{R}$, $\mathbb{R}_r$, $\mathbb{R}$	Pose deviation, actual pose matrix, nominal pose matrix
A	Jacobian matrix of the error model.
$\Delta\xi$	Kinematic parameters error vector.
$\Delta\alpha$, Δa, Δd ,$\Delta\theta$	Vector of the kinematic parameter deviations.
M	Sample count (measurement configurations).
C, $\hat{C}$	Cable measured length, cable nominal length.
S_0	Fixed point coordinate on the ground.
S_i	Nominal position coordinate.
$\{q_{i,1}, \ldots, q_{i,6}\}$	Torsion angles.
f	Objective function.
$\hat{A}$	Error extended Jacobian matrix.
Z, $\hat{Z}$	Orthogonal matrices.
Λ	Diagonal matrix.
z	Dimension of the D-H parameter vector.
$(\sigma_1, \sigma_2, \cdots, \sigma_z)$	Singular values of the matrix Λ.
$O_1, \ldots, O_6$,	Observability indices
m	Selected sample count (measurement configurations selected by MCS)
u	D-H parameter vector.
Λ_k	Regularized constant.
a_6	Link length of the robot's sixth axis.
$\hat{a}_6$	Defined link length of the robot's sixth axis.
D	Length of the dial indicator.
$\hat{D}$	Dial indicator reading.
ψ_k	Constraint equation of plane k.
G_k	A point of plane k.
η_j	Normal vector of plane k.
n	Total number of planes.
ρ_k	Constraint factor for plane k.
Υ_k	Lagrange multiplier of plane k.
$<\cdot>$	Inner product between two matrices.
I	Unit matrix.
l_k	Distance from the point on the plane k to the industrial robot coordinate origin.
τ_k	Step size of the Lagrange multiplier of the plane k.
a_1	An element of w.
B_i	Measured position.
K_1, K_2, K_3	Max iteration's round.

TABLE S.II. HRS JR680 industrial robot D-H parameters.

No.	a_i/mm	θ_i/°	α_i/°	d_i/mm
Joint 1	250	0	-90	653.5
Joint 2	900	-90	0	0
Joint 3	-205	180	-90	0
Joint 4	0	0	90	1030.2
Joint 5	0	90.0	-90	0
Joint 6	0	0	0	200.6

TABLE S.II. TECHNICAL INDICATORS OF THE DRAWSTRING DISPLACEMENT SENSOR.

Items	Technical indicators
Maximum measuring length	2000 mm
Resolution	0.004mm
Operating voltage	DC 5-24V
Maximum rate	1000m/s
Linearity	0.05%FS
Ambient temperature	-25℃~85℃

TABLE S.III. TECHNICAL INDICATORS OF THE DRAWSTRING DISPLACEMENT INDICATOR.

Items	Technical indicators
Input resistance	5K
Amplification range	0~999.999
Operating voltage	AC220V 50Hz
Pulse length	2μs
Linearity	0.05%FS
Ambient temperature	-10℃~50℃

TABLE S.IV. TECHNICAL INDICATORS OF THE DIAL INDICATOR.

Items	Technical indicators
Range	12.7mm
Resolution	0.001mm
Power supply	3V lithium battery CR2032
Data output	Rs232
Ambient temperature	0℃~40℃

TABLE S.IV. TECHNICAL INDICATORS OF THE HIGH-PRECISION MARBLE GAUGE BLOCK.

Items	Technical indicators
Precision grade	Class 00/0.003mm
Size	400mm×300mm×70mm
Compressive strength	240N/m~245N/m
Data output	Rs232
Shore hardness	>HS70

TABLE S.V. TECHNICAL INDICATORS OF THE HRS JR680 INDUSTRIAL ROBOT.

Items	Technical indicators
Maximum working radius	2200mm
Degrees of freedom	6
Repeatability	±0.07mm
Rated Power/Voltage/Current	8.8kW/3-phase AC 380V/16.8A
Protection rating	IP54/ IP65 (wrist)
Robot weight	720kg
Rated load	80kg
Ambient temperature	0℃~45℃

TABLE S.VI. CALIBRATION ACCURACY OF THE AMPC ALGORITHM FOR DIFFERENT SAMPLE SIZES IN D1-3.

Sample sizes	D1			D2			D3		
	RMSE/mm	MEAN/mm	MAX/mm	RMSE/mm	MEAN/mm	MAX/mm	RMSE/mm	MEAN/mm	MAX/mm
S100	$0.623_{\pm 2.1E-2}$	$0.523_{\pm 1.9E-2}$	$1.005_{\pm 2.9E-2}$	$0.618_{\pm 2.6E-2}$	$0.518_{\pm 2.1E-2}$	$0.995_{\pm 2.9E-2}$	$0.630_{\pm 2.2E-2}$	$0.532_{\pm 2.2E-2}$	$1.021_{\pm 2.8E-2}$
S200	$0.594_{\pm 1.9E-2}$	$0.492_{\pm 1.8E-2}$	$0.965_{\pm 1.9E-2}$	$0.590_{\pm 1.5E-3}$	$0.488_{\pm 1.7E-2}$	$0.955_{\pm 1.6E-2}$	$0.606_{\pm 1.5E-2}$	$0.505_{\pm 3.1E-2}$	$0.982_{\pm 5.5E-2}$
S300	$0.592_{\pm 1.2E-2}$	$0.490_{\pm 1.2E-2}$	$0.963_{\pm 1.6E-2}$	$0.588_{\pm 4.0E-2}$	$0.486_{\pm 1.0E-2}$	$0.953_{\pm 1.1E-2}$	$0.603_{\pm 1.2E-2}$	$0.503_{\pm 3.8E-2}$	$0.980_{\pm 5.3E-2}$
S500	$0.591_{\pm 1.0E-2}$	$0.489_{\pm 1.1E-2}$	$0.961_{\pm 1.0E-2}$	$0.587_{\pm 9.2E-3}$	$0.485_{\pm 9.3E-3}$	$0.952_{\pm 8.3E-2}$	$0.602_{\pm 7.0E-3}$	$0.502_{\pm 7.1E-3}$	$0.979_{\pm 1.6E-2}$
S700	$0.590_{\pm 3.8E-3}$	$0.488_{\pm 4.6E-3}$	$0.960_{\pm 5.1E-3}$	$0.586_{\pm 2.6E-3}$	$0.484_{\pm 2.2E-3}$	$0.951_{\pm 3.1E-3}$	$0.601_{\pm 2.3E-2}$	$0.501_{\pm 3.0E-3}$	$0.978_{\pm 2.4E-3}$

TABLE S.VII. TOTAL TIME COSTS OF THE AMPC ALGORITHM FOR DIFFERENT SAMPLE SIZES IN D1-3.

Sample size	D1		D2		D3	
	Iterations	Time/s	Iterations	Time/s	Iterations	Time/s
S100	19	**$21.3_{\pm 0.97}$**	19	**$22.0_{\pm 0.76}$**	28	**$25.8_{\pm 0.81}$**
S200	11	$22.7_{\pm 0.83}$	13	$27.0_{\pm 0.75}$	15	$28.2_{\pm 0.80}$
S300	11	$29.3_{\pm 0.62}$	12	$32.7_{\pm 0.73}$	14	$34.5_{\pm 0.72}$
S500	10	$41.1_{\pm 0.57}$	11	$42.9_{\pm 0.58}$	14	$49.7_{\pm 0.65}$
S700	10	$53.6_{\pm 0.53}$	11	$55.2_{\pm 0.57}$	13	$63.8_{\pm 0.56}$

TABLE S.VIII. CALIBRATION ACCURACY OF ALGORITHMS M1-9 ON P1-3.

Algorithms	P1			P2			P3		
	RMSE/mm	MEAN/mm	MAX/mm	RMSE/mm	MEAN/mm	MAX/mm	RMSE/mm	MEAN/mm	MAX/mm
Before	2.562	2.451	4.510	2.562	2.451	4.510	2.562	2.451	4.510
M1	$0.979_{\pm 5.2E-2}$	$0.878_{\pm 4.8E-2}$	$1.755_{\pm 4.9E-2}$	$0.930_{\pm 3.6E-2}$	$0.824_{\pm 3.2E-2}$	$1.702_{\pm 2.9E-2}$	$0.921_{\pm 2.2E-2}$	$0.803_{\pm 2.2E-2}$	$1.686_{\pm 2.8E-2}$
M2	$1.252_{\pm 3.3E-2}$	$1.162_{\pm 3.8E-2}$	$2.425_{\pm 6.5E-2}$	$1.195_{\pm 9.1E-3}$	$1.108_{\pm 1.0E-2}$	$2.375_{\pm 1.1E-2}$	$1.182_{\pm 3.2E-2}$	$1.066_{\pm 3.1E-2}$	$2.293_{\pm 5.5E-2}$
M3	$0.653_{\pm 0.5E-0}$	$0.573_{\pm 0.3E-0}$	$1.125_{\pm 0.6E-0}$	$0.601_{\pm 0.2E-2}$	$0.510_{\pm 0.7E-2}$	$1.094_{\pm 0.3E-2}$	$0.587_{\pm 0.2E-2}$	$0.503_{\pm 0.6E-2}$	$1.035_{\pm 0.1E-2}$
M4	$0.772_{\pm 5.9E-3}$	$0.673_{\pm 5.9E-3}$	$1.522_{\pm 5.0E-2}$	$0.712_{\pm 4.0E-2}$	$0.612_{\pm 4.0E-2}$	$1.460_{\pm 5.1E-2}$	$0.673_{\pm 4.6E-2}$	$0.572_{\pm 3.8E-2}$	$1.406_{\pm 5.3E-2}$
M5	$1.068_{\pm 4.0E-2}$	$0.887_{\pm 3.9E-2}$	$1.858_{\pm 3.2E-2}$	$1.030_{\pm 2.8E-2}$	$0.818_{\pm 3.1E-2}$	$1.808_{\pm 3.2E-2}$	$1.023_{\pm 3.2E-2}$	$0.812_{\pm 3.3E-2}$	$1.793_{\pm 6.9E-2}$
M6	$0.698_{\pm 1.3E-0}$	$0.597_{\pm 1.1E-0}$	$1.321_{\pm 1.0E-0}$	$0.643_{\pm 5.2E-3}$	$0.541_{\pm 2.8E-3}$	$1.279_{\pm 2.2E-2}$	$0.629_{\pm 2.0E-2}$	$0.525_{\pm 7.1E-3}$	$1.255_{\pm 1.6E-2}$
M7	$1.111_{\pm 5.8E-2}$	$1.012_{\pm 4.9E-2}$	$2.101_{\pm 6.3E-2}$	$1.060_{\pm 5.3E-2}$	$0.965_{\pm 4.9E-2}$	$2.054_{\pm 5.0E-2}$	$1.052_{\pm 4.0E-2}$	$0.950_{\pm 3.2E-2}$	$2.030_{\pm 5.2E-2}$
M8	$0.594_{\pm 1.9E-2}$	$0.492_{\pm 1.8E-2}$	$0.965_{\pm 1.9E-2}$	$0.565_{\pm 1.9E-2}$	$0.465_{\pm 1.8E-2}$	$0.913_{\pm 1.9E-2}$	$0.551_{\pm 5.8E-2}$	$0.451_{\pm 4.0E-2}$	$0.890_{\pm 4.0E-2}$
M9	$0.549_{\pm 1.8E-2}$	$0.449_{\pm 1.6E-2}$	$0.885_{\pm 9.1E-3}$	$0.528_{\pm 9.2E-3}$	$0.423_{\pm 8.2E-3}$	$0.829_{\pm 6.1E-3}$	**$0.502_{\pm 2.3E-3}$**	**$0.411_{\pm 3.0E-3}$**	**$0.815_{\pm 2.4E-3}$**

TABLE S.IX. TOTAL TIME COSTS OF ALGORITHMS M1-9 ON P1-3.

Datasets	Items	M1	M2	M3	M4	M5	M6	M7	M8	M9
P1	Iteration	26	12	50	85	16	65	13	11	2
	Time/s	$75.2_{\pm 0.53}$	$22.0_{\pm 1.72}$	$108.0_{\pm 0.26}$	$42.1_{\pm 0.82}$	$30.0_{\pm 3.12}$	$122.6_{\pm 0.32}$	$19.0_{\pm 0.10}$	$22.7_{\pm 0.83}$	$43.3_{\pm 0.11}$
P2	Iteration	25	12	49	82	16	65	13	11	2
	Time/s	$130.1_{\pm 0.93}$	$42.1_{\pm 1.02}$	$192.6_{\pm 1.06}$	$80.9_{\pm 2.02}$	$59.2_{\pm 3.69}$	$228.52_{\pm 0.53}$	$38.9_{\pm 0.53}$	$42.6_{\pm 1.20}$	$54.2_{\pm 0.23}$
P3	Iteration	23	12	49	79	15	63	12	10	**2**
	Time/s	$202.1_{\pm 1.21}$	$65.2_{\pm 1.02}$	$289.3_{\pm 0.99}$	$120.2_{\pm 3.89}$	$82.16_{\pm 3.52}$	$328.6_{\pm 0.59}$	$63.6_{\pm 0.38}$	$65.3_{\pm 1.98}$	**$62.8_{\pm 0.23}$**

TABLE S.X. WILCOXON SIGNED RANKS TEST ON RMSE/MEAN/MAX OF TABLE S. III.

Comparison	*R-*	*R+*	*p-value*
M9 vs. M1	0	45	0.002
M9vs. M2	0	45	0.002
M9 vs. M3	0	45	0.002
M9 vs. M4	0	45	0.002
M9 vs. M5	0	45	0.002
M9 vs. M6	0	45	0.002
M9 vs. M7	0	45	0.002
M9 vs. M8	0	45	0.002

*Highlighted are the hypotheses that are accepted at a significance level of 0.05.

TABLE S.XI. EIGHT VECTORS OF D-H PARAMETER VECTORS ON P3 AFTER BEING CALIBRATED BY M9.

D-H Parameters	Joints	DH1	DH2	DH3	DH4	DH5	DH6	DH7
a_i/mm	1	249.8875	249.8875	249.8876	249.8876	249.8875	249.8874	249.8876
	2	897.8369	897.8369	897.8370	897.8370	897.8369	897.8368	897.8370
	3	-203.6448	-203.6448	-203.6448	-203.6448	-203.6448	-203.6448	-203.6449
	4	0.6372	0.6372	0.6372	0.6372	0.6372	0.6372	0.6371
	5	-0.2672	-0.2672	-0.2672	-0.2673	-0.2672	-0.2672	-0.2673
	6	-0.0681	-0.0681	-0.0681	-0.0680	-0.0681	-0.0681	-0.0680
d_i/mm	1	654.3120	654.3118	654.3115	654.3113	654.3122	654.3125	654.311
	2	-0.6389	-0.6389	-0.6389	-0.6389	-0.6389	-0.6389	-0.6389
	3	-0.2377	-0.2377	-0.2377	-0.2377	-0.2377	-0.2377	-0.2377
	4	1032.4214	1032.4214	1032.4214	1032.4214	1032.4214	1032.4214	1032.4214
	5	0.3221	0.3221	0.3220	0.322	0.3221	0.3222	0.3219
	6	200.0263	200.0261	200.0258	200.0256	200.0265	200.0268	200.0254
$\alpha_i/^\circ$	1	-90.2133	-90.2075	-90.2018	-90.1962	-90.2192	-90.2253	-90.1907
	2	-0.0156	-0.0106	-0.0057	-0.0010	-0.0208	-0.0262	0.0036
	3	-89.9755	-89.9736	-89.9717	-89.9699	-89.9775	-89.9796	-89.9681
	4	89.9965	89.9982	89.9999	90.0015	89.9947	89.9929	90.0031
	5	-89.9643	-89.9644	-89.9646	-89.9647	-89.9642	-89.964	-89.9648
	6	0.0965	0.0965	0.0965	0.0965	0.0965	0.0965	0.0965
$\theta_i/^\circ$	1	0.0157	0.0064	-0.0026	-0.0115	0.0252	0.0349	-0.0202
	2	-90.0535	-90.0586	-90.0636	-90.0687	-90.0484	-90.0434	-90.0738
	3	180.0862	180.0869	180.0875	180.0881	180.0855	180.0847	180.0887
	4	0.0653	0.0645	0.0637	0.0630	0.0661	0.0669	0.0622
	5	90.0032	90.0030	90.0029	90.0027	90.0034	90.0035	90.0025
	6	0.0026	0.0028	0.0029	0.0031	0.0024	0.0023	0.0033

TABLE S.XII. CALIBRATION ACCURACY OF DH1-7 ON P3.

D-H Parameters	RMSE/mm	MEAN/mm	MAX/mm
DH1	0.502	0.411	0.815
DH2	0.501	0.409	0.813
DH3	0.503	0.412	0.816
DH4	0.499	0.408	0.812
DH5	0.500	0.410	0.814
DH6	0.504	0.413	0.817
DH7	0.505	0.414	0.818

TABLE S.XIII. CALIBRATION ACCURACY OF E1-7 ON P3.

Ensembles	RMSE/mm	MEAN/mm	MAX/mm
E1	0.497	0.407	0.810
E2	0.494	0.404	0.806
E3	0.491	0.402	0.803
E4	0.489	0.401	0.801
E5	0.488	0.400	0.800
E6	0.488	0.400	0.800

TABLE S.XIV. THE D-H PARAMETER DEVIATIONS OF THE E5 ENSEMBLE ON P3.

Joints	Δa_i/°	Δa_i/mm	Δd_i/mm	$\Delta \theta_i$/°
1	-0.1958	-0.1124	0.8112	-0.0122
2	-0.0007	-2.1630	-0.6389	-0.0692
3	0.0303	1.3552	-0.2377	0.0881
4	0.0016	0.6372	2.2214	0.0629
5	0.0353	-0.2673	0.3220	0.0027
6	0.0965	-0.0680	-0.5744	0.0031

II. ADDITIONAL ALGORITHM PSEUDOCODE

Algorithm I: MCS-AMPC Calibrator

Input: w_0, z, K_1, K_2, K_3, M, $\{q_{i,1}, q_{i,2}, \ldots, q_{i,6}\}$, $\{C_1, C_2, \ldots, C_M\}$, $G_{0,k}$, $\eta_{0,k}$, $\Upsilon_{0,k}$, n, S_0

Operation	**Cost**
/* Initialization */	
1. **initialize** n=3, λ_k, v=2, ρ_k	T_1
2. **initialize** w=w_0, G_k=$G_{0,k}$, η_k=$\eta_{0,k}$, Υ_k=$\Upsilon_{0,k}$, S_0	
/* MCS Step*/	
3. **for** t= z to N_0	
4. g=t	
5. **calculate** O_6 via **Algorithm II**	
6. **end for**	
7. **output** m according to the observability indices	
8. **for** t_1=1 to K_1	T_2
9. **generate** m configurations randomly from M configurations	
10. s=m	
11. **calculate** O_6 via **Algorithm II**	
12. **building** the MCS based on the updated rules of the DE algorithm	
13. **end for**	
Output m measurement configurations (the best group of samples)	
/* AMPC Step */	
Input the best group of samples	
21. **for** t_2=1 to K_2	
22. **for** i=1 to m	
23. **update** $S_{0,t+1}$ with (17)	
25. **end for**	
26. **end for**	
27. **for** t_3=1 to K_3	
28. **for** i=1 to m	T_3
29. **update** $G_{k,t+1}$, and $\eta_{k,t+1}$ with (18) and (19)	
30. **update** w_{t+1} with (21)	
31. **update** $\Upsilon_{j,t+1}$ with (22)	
32. **normalize** $G_{j,t+1}$, and $\eta_{j,t+1}$ with (20)	
33. **end for**	
34. **end for**	
/* Operation Ending */	
Output: w	

Algorithm II: Calculation of O_6

Input: w_0, g, $\{q_{i,1}, q_{i,2}, \ldots, q_{i,6}\}$,

Operation	**Cost**
/* Initialization */	
1. **Initialize** u=u_0, g	T_{21}
/*MCS Step*/	
2. **for** i=1 to g	
3. **calculate** the A with (5)	
4. **end for**	
5. **computing** $\hat{A}$ based on (8)	T_{22}
6. **update** σ_1-σ_z with (9) and (10)	
7. **updating** O_6 based on (11)	
/* Operation Ending */	
Output: O_6	

III. ADDITIONAL FIGURES

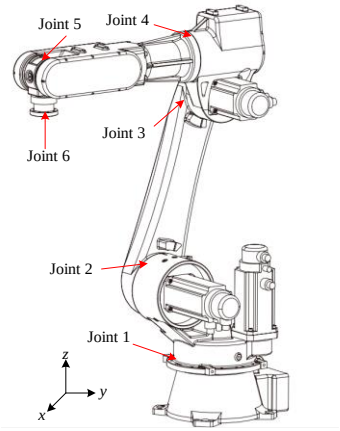

Fig. S.1. The HSR-JR680 industrial robot. The picture originates from this website (https://www.hsrobotics.cn/download.php).

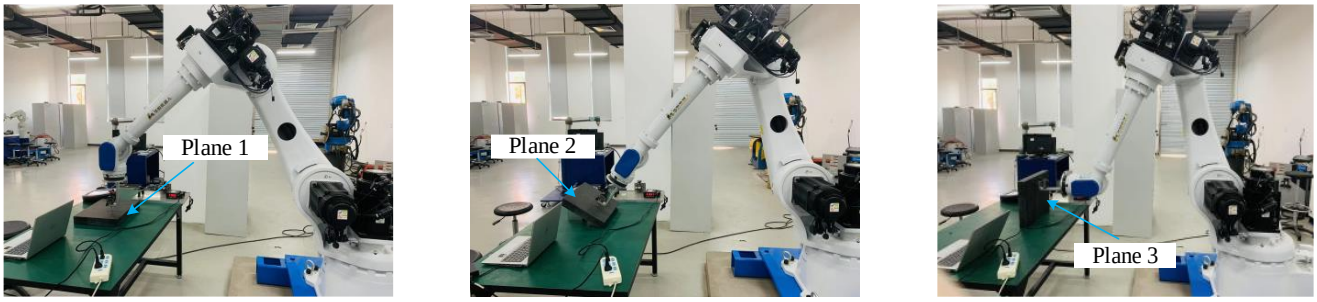

(a) (b) (c)

Fig. S.2. The samples collection process on D1-3. (a), (b) and (c) correspond to D1-3, respectively.

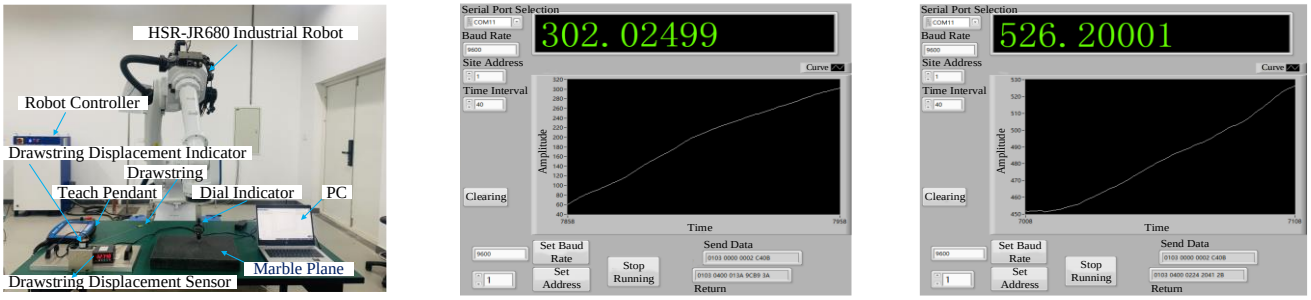

(a) (b) (c)

Fig. S.3. The experimental system. (a) The experimental platform, (b) and (c) The LabVIEW software on two different samples.

(a) (b) (c)

Fig. S.4. The measurement configuration collection process on D1. In this process, three measurement configurations are utilized as examples, with three points preset on the plane. Since the dial gauge is fixed at the end of the robot, the robot's movement is controlled so that the dial gauge sequentially touches three selected points on the plane, gathering data for each point. (a) Robot's pose for collecting measurement configuration 1. (b) Robot's pose for collecting measurement configuration 2. (c) Robot's pose for collecting measurement configuration 3.

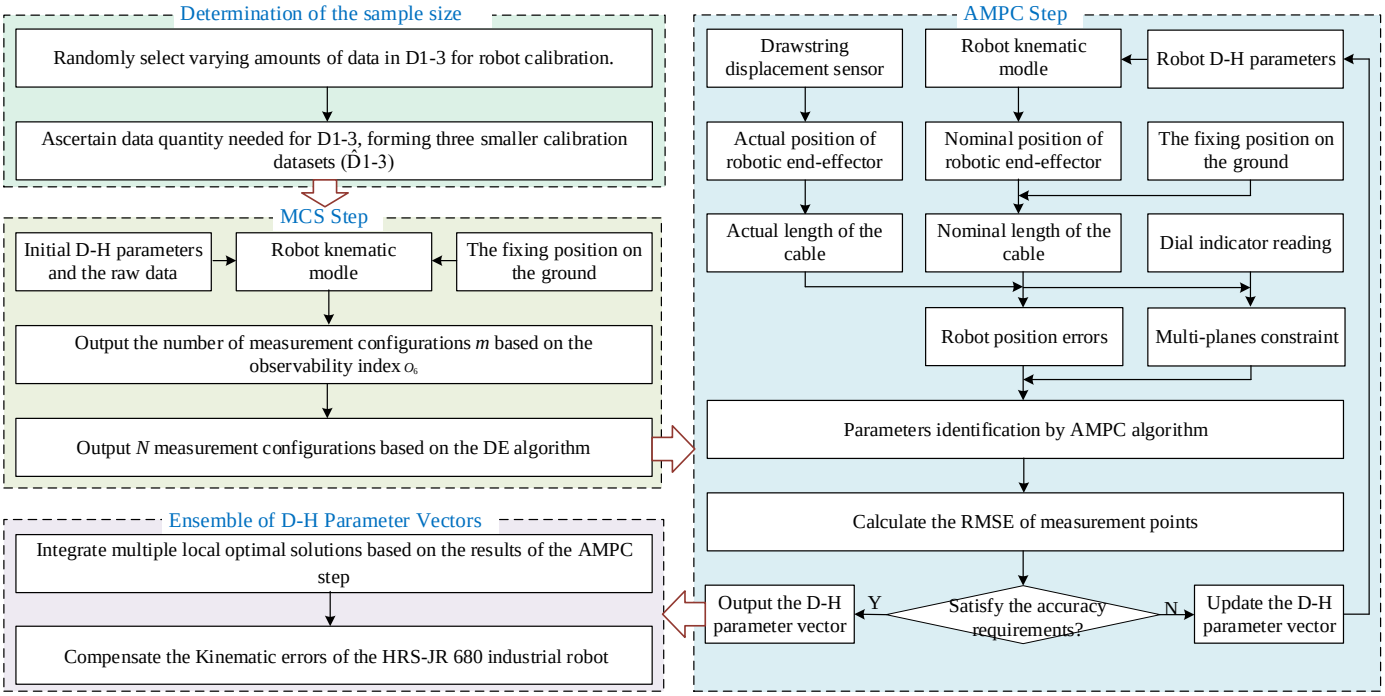

Fig. S.5. The calculation process of robot calibration.

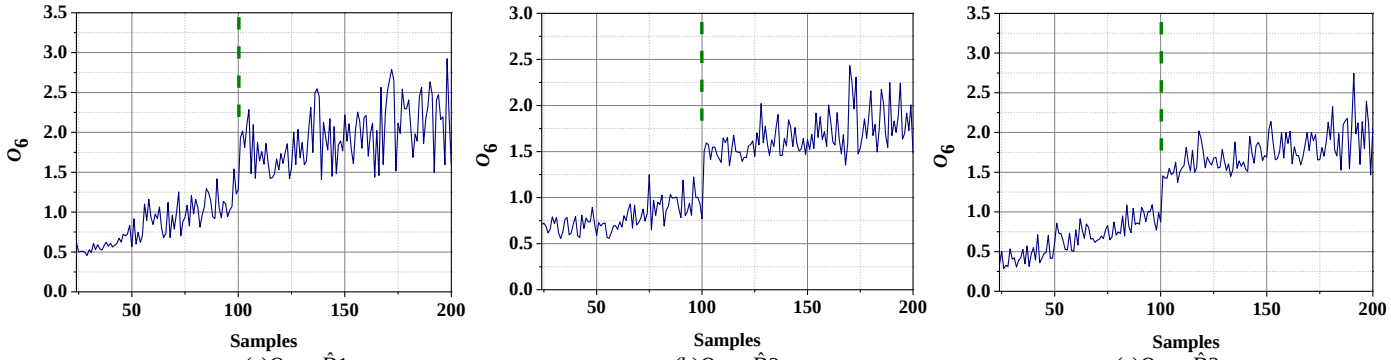

(a)O_6 on D̂1 (b)O_6 on D̂2 (c)O_6 on D̂3

Fig. S.6. The number of measurement configurations affecting O6 on D̂1-3.

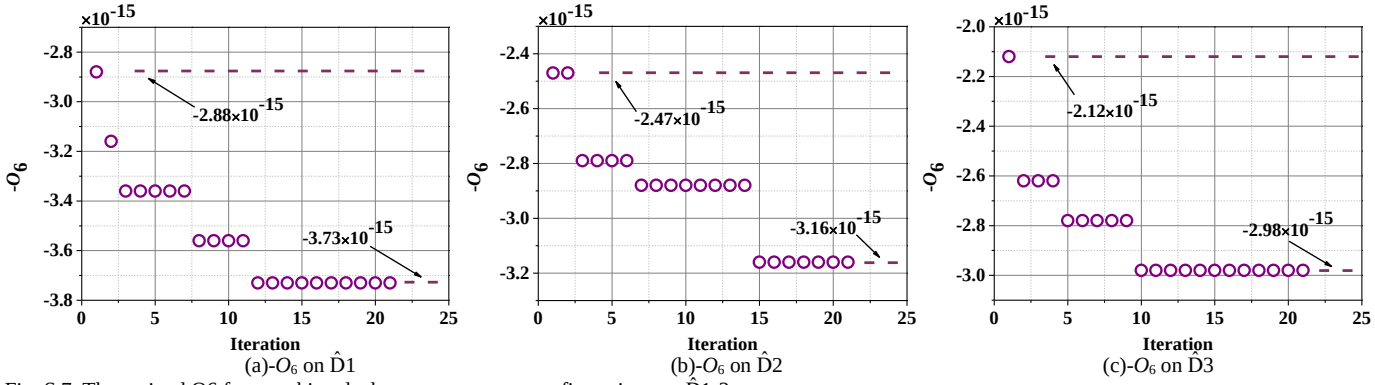

(a)-O_6 on D̂1 (b)-O_6 on D̂2 (c)-O_6 on D̂3

Fig. S.7. The optimal O6 for searching the best measurement configurations on D̂1-3.

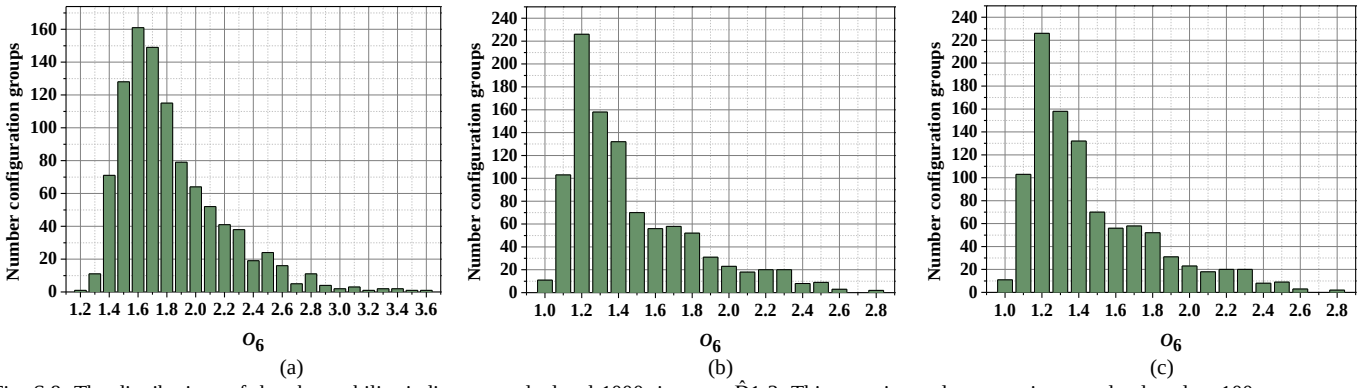

Fig. S.8. The distributions of the observability indices are calculated 1000 times on $\hat{D}$1-3. This experimental propose is to randomly select 100 measurement configurations in 200 samples.

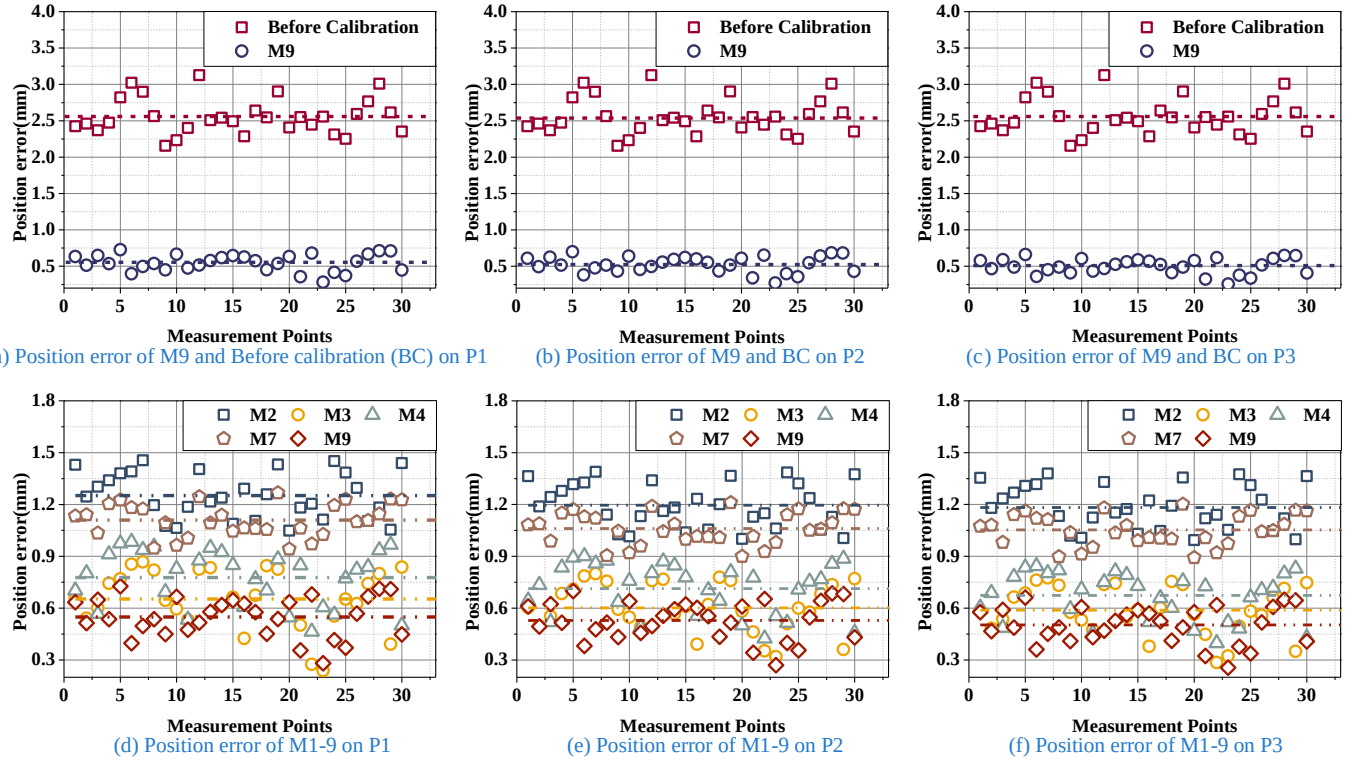

(a) Position error of M9 and Before calibration (BC) on P1
(b) Position error of M9 and BC on P2
(c) Position error of M9 and BC on P3
(d) Position error of M1-9 on P1
(e) Position error of M1-9 on P2
(f) Position error of M1-9 on P3

Fig. S.9. The position error of the industrial robot after calibration using various algorithms on P1-3. Note that the dotted lines represent the average values. Panels (a)-(c) illustrate that the industrial robot obtains an evident enhancement of position accuracy after calibration. Panels (d)-(f) show that M9 has the best position accuracy when compared to M1-8.

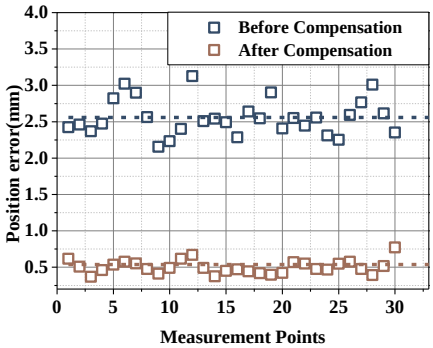

Fig. S.10. The position error of the industrial robot before and after compensation on HRS-AC. Note that the dotted lines represent the average values. The results show that after D-H parameter compensation, the position accuracy of the industrial robot is effectively improved.

IV. Convergence Analysis of AMPC

Given nodes $i \in m$, and iteration t, the convergence is divided into two sequential steps:
Step 1. The difference between Υ_{t+1} and Υ_t is bounded by that between (η_{t+1}, G_{t+1}, $a_{1,t+1}$) and (η_t, G_t, $a_{1,t}$);
Step 2. The augmented Lagrangian function (23) is non-increasing and low-bounded.

A. Proof of Step 1

This work provides proof with Γ as an active variable. Thus, *Lemma* 1 is presented as:
Lemma 1: With (29), $(\Upsilon_{t+1}\text{-}\Upsilon_t)^2$ is bounded by:

$$\left(\Upsilon_{t+1}-\Upsilon_t\right)^2 \le 2\left(\rho\left(\tau-1\right)\right)^2\left(\frac{1}{m}\sum_{i=1}^{m}\left(\Psi_i\left(a_{t+1},G_{t+1},\eta_{t+1}\right)-\Psi_i\left(a_t,G_t,\eta_t\right)\right)\right)^2+2\left(\frac{1}{m}\sum_{i=1}^{m}\left(\frac{1}{\kappa_{2,i,t+1}}\left(a_{1,t+1}+\kappa_{1,i,t+1}\right)-\frac{1}{\kappa_{2,i,t}}\left(a_{1,t}+\kappa_{1,i,t}\right)\right)\right)^2=\nu_\Upsilon. \tag{S1}$$

Proof: Consider that (23) is non-convex, implying that any equilibrium point having a zero-gradient (e.g., a saddle point or a global/local optimum) has the potential to be a feasible solution. Given the solution to a_1 by (29c) to be $a_{1,t+1}$, yielding:

$$\Upsilon_t+\frac{1}{m}\sum_{i=1}^{m}\left(\frac{1}{\kappa_{2,i,t+1}}\left(a_{1,t+1}+\kappa_{1,i,t+1}\right)+\rho\cdot\Psi\left(a_{t+1},G_{t+1},\eta_{t+1}\right)\right)=0. \tag{S2}$$

By replacing the values of Υ derived from equations (27d) and (29d) into expression (S2), we can derive:

$$\Upsilon_{t+1}=\left(\tau-1\right)\frac{\rho}{m}\sum_{i=1}^{m}\Psi_i\left(a_{1,t+1},G_{t+1},\eta_{t+1}\right)-\frac{1}{m}\sum_{i=1}^{m}\frac{1}{\kappa_{2,i,t+1}}\left(a_{1,t+1}+\kappa_{1,i,t+1}\right)=0. \tag{S3}$$

Hence, the difference between Υ_{t+1} and Υ_t is given as:

$$\Upsilon_{t+1}-\Upsilon_t=\left(\tau-1\right)\frac{\rho}{m}\sum_{i=1}^{m}\left(\Phi_i\left(a_{1,t+1},G_{t+1},\eta_{t+1}\right)-\Phi_i\left(a_{1,t},G_t,\eta_t\right)\right)-\frac{1}{m}\sum_{i=1}^{m}\left(\frac{1}{\kappa_{2,i,t+1}}\left(a_{1,t+1}+\kappa_{1,i,t+1}\right)-\frac{1}{\kappa_{2,i,t}}\left(a_{1,t}+\kappa_{1,i,t}\right)\right). \tag{S4}$$

With the inequality $(x\text{-}y)^2 \le 2(x^2+y^2)$, (S1) is fulfilled. Thus, *Lemma* 1 stands to implement Step 1.

B. Proof of Step 2

To facilitate the execution of Step 2, we present *Lemma* 2:
Lemma 2: If the following criteria are fulfilled:

$$\rho\le 0,\ \ \tau\ge 0,\ \ \eta_{x,t}\ge 0,\ \ \eta_{y,t}\ge 0,\ \ \eta_{z,t}\ge 0, \tag{S5a}$$

$$\frac{1}{\kappa_{2,i,t+1}}\left(a_{1,t+1}+\kappa_{1,i,t+1}\right)\le 0,\ \ \tau\ge\frac{1}{2}, \tag{S5b}$$

the following inequality stands:

$$f\left(\eta_{t+1},G_{t+1},a_{1,t+1},\Upsilon_{t+1}\right)-f\left(\eta_t,G_t,a_{1,t},\Psi_t\right)\le 0, \tag{S6a}$$

$$f\left(\eta_{t+1},G_{t+1},a_{1,t+1},\Upsilon_{t+1}\right)\ge 0. \tag{S6b}$$

Proof: Considering the second-order Taylor expansion of f at the point of (γ_{t+1}, W_t, $a_{1,t}$ and Γ_t), we have:

$$f\left(\eta_{t+1},G_t,a_{1,t},\Upsilon_t\right)-f\left(\eta_t,G_t,a_{1,t},\Upsilon_t\right)\overset{(27a),(29a)}{=}\frac{\rho}{2m}\sum_{i=1}^{m}\begin{bmatrix}\kappa_{4,i,t}^2\left(\eta_{x,t+1}-\eta_{x,t}\right)^2+\kappa_{5,i,t}^2\left(\eta_{y,t+1}-\eta_{y,t}\right)^2\\+\kappa_{6,i,t}^2\left(\eta_{z,t+1}-\eta_{z,t}\right)^2\end{bmatrix}. \tag{S7}$$

Note that based on optimal conditions in (27a) and (29a), the first-order term is zero and has been omitted for brevity. Likewise, the difference between $f(\eta_{t+1}, G_{t+1}, a_{1,t}$ and $\Upsilon_t)$ and $f(\eta_{t+1}, G_t, a_{1,t}$ and $\Upsilon_t)$, and $f(\eta_{t+1}, G_{t+1}, a_{1,t+1}$ and $\Upsilon_t)$ and $f(\eta_{t+1}, G_{t+1}, a_{1,t}$ and $\Upsilon_t)$ can be formulated by:

$$f\left(\eta_{t+1},G_{t+1},a_{1,t},\Upsilon_t\right)-f\left(\eta_{t+1},G_t,a_{1,t},\Upsilon_t\right)\overset{(27b),(29b)}{=}\frac{\rho}{2m}\sum_{t=1}^{m}\left(\eta_{x,t+1}\left(G_{x,t+1}-G_{x,t}\right)^2+\eta_{y,t+1}\left(G_{y,t+1}-G_{y,t}\right)^2+\eta_{z,t+1}\left(G_{z,t+1}-G_{z,t}\right)^2\right), \tag{S8}$$

$$f\left(\eta_{t+1},G_{t+1},a_{1,t+1},\Upsilon_t\right)-f\left(\eta_{t+1},G_{t+1},a_{1,t},\Upsilon_t\right)\overset{(27c),(29c)}{=}\frac{1}{2m}\sum_{i=1}^{m}\left(1+\rho\kappa_{2,i,t}^2\right)\left(a_{1,t+1}-a_{1,t}\right)^2. \tag{S9}$$

Additionally, $f(\eta_{t+1}, G_{t+1}, a_{1,\,t+1}$ and $\Upsilon_{t+1})$ and $f(\eta_{t+1}, G_{t+1}, a_{1,\,t+1}$ and $\Upsilon_t)$ are differed as:

$$f\left(\eta_t,G_{t+1},a_{1,t+1},\Upsilon_{t+1}\right)-f\left(\eta_t,G_t,a_{1,t},\Upsilon_t\right)\overset{(27d),(29d)}{=}\frac{\left(\Upsilon_{t+1}-\Upsilon_t\right)^2}{\tau\rho}\overset{S1}{\le}\frac{\nu_\Upsilon}{\tau\rho}. \tag{S10}$$

With (S9), the equality can be deduced from the update rules (27d) and (29d), whereas the inequality is contingent upon the premises established in Lemma 1. Through a logical combination of equations (S7) to (S10), the following result can be inferred:

$$
\begin{aligned}
&f\left(\eta_t, G_{t+1}, a_{1,t+1}, \Upsilon_{t+1}\right) - f\left(\eta_t, G_t, a_{1,t}, \Upsilon_t\right) \le \frac{\rho}{2m}\sum_{i=1}^{m}\left(\kappa_{4,i,t}^2\left(\eta_{x,t+1}-\eta_{x,t}\right)^2 + \kappa_{5,i,t}^2\left(\eta_{y,t+1}-\eta_{y,t}\right)^2 + \kappa_{6,i,t}^2\left(\eta_{z,t+1}-\eta_{z,t}\right)^2\right) \\
&+\frac{\rho}{2m}\sum_{i=1}^{m}\left(\eta_{x,t}\left(G_{x,t+1}-G_{x,t}\right)^2 + \eta_{y,t}\left(G_{y,t+1}-G_{y,t}\right)^2 + \eta_{z,t}\left(G_{z,t+1}-G_{z,t}\right)^2\right)^2 + \frac{1}{2m}\sum_{i=1}^{m}\left(1+\rho\kappa_{2,i,t}^2\right)\left(a_{1,t+1}-a_{1,t}\right)^2 \\
&+\frac{2}{\tau}\left(\tau-1\right)^2\rho\frac{1}{m}\sum_{i=1}^{m}\left(\Phi_i\left(a_{t+1}, G_{t+1}, \eta_{t+1}\right) - \Phi_i\left(a_t, G_t, \eta_t\right)\right)^2 + 2\frac{1}{\rho\tau}\left(\frac{1}{m}\sum_{i=1}^{m}\left(\frac{1}{\kappa_{2,i,t+1}}\left(a_{1,t+1}+\kappa_{1,i,t+1}\right) - \frac{1}{\kappa_{2,i,t}}\left(a_{1,t}+\kappa_{1,i,t}\right)\right)\right)^2 \le 0, \qquad \text{(S11)} \\
&\Rightarrow \rho \le 0, \eta_{x,t} \ge 0, \eta_{y,t} \ge 0, \eta_{z,t} \ge 0, \frac{2}{\tau}\left(\tau-1\right)^2\rho \le 0, \frac{1}{\rho\tau} \le 0, \\
&\Rightarrow \rho \le 0, \eta_{x,t} \ge 0, \eta_{y,t} \ge 0, \eta_{z,t} \ge 0, \tau \ge 0.
\end{aligned}
$$

Hence, (S5a) and (S6a) are fulfilled, which demonstrates that (23) is non-increasing in this case. After (*t*+1)-*th* iteration, (23) can be reformulated as:

$$
f\left(\eta_{t+1}, G_{t+1}, a_{1,t+1}, \Upsilon_{t+1}\right) = \frac{1}{2m}\sum_{i=1}^{m}\left\|B_i - \hat{C}_i\right\|_2^2 + \frac{1}{m}\sum_{i=1}^{m}\left\langle\Psi_i\left(a_{1,t+1}, G_{t+1}, \eta_{t+1}\right), \Upsilon_{t+1}\right\rangle + \frac{1}{2m}\sum_{i=1}^{m}\rho\left\|\Psi_i\left(a_{1,t+1}, G_{t+1}, \eta_{t+1}\right)\right\|_2^2. \qquad \text{(S12)}
$$

By substituting (S3) into (S11), we can obtain:

$$
f\left(\eta_{t+1}, G_{t+1}, a_{1,t+1}, \Upsilon_{t+1}\right) = \frac{1}{2m}\sum_{i=1}^{m}\left\|B_i - \hat{C}_i\right\|_2^2 + \frac{\left(2\tau-1\right)\rho}{2}\frac{1}{m}\sum_{i=1}^{m}\left(\Phi_i\left(a_{1,t+1}, G_{t+1}, \eta_{t+1}\right)\right)^2 - \frac{1}{m}\sum_{i=1}^{m}\frac{1}{\kappa_{2,i,t+1}}\left(a_{1,t+1}+\kappa_{1,i,t+1}\right). \qquad \text{(S13)}
$$

With (S5b) and (S13), (S6b) is fulfilled, i.e., (23) is lower-bounded. Hence, *Lamma* 2 stands, making Step 2 complete. To sum up, as per the aforementioned deductions, with the implementation of Steps 1 through 2, AMPC's convergence can be established with certainty in theory.